International Journal of Heat and Mass Transfer 52 (2009) 4184–4194

Contents lists available at ScienceDirect

International Journal of Heat and Mass Transfer

journal homepage: www.elsevier.com/locate/ijhmt

Carbon dioxide local heat transfer coefficients during flow boiling in a horizontal circular smooth tube

R. Mastrullo [a], A.W. Mauro [a], A. Rosato [a,*], G.P. Vanoli [b]

[a] D.E.TE.C., Facoltà di Ingegneria, Università degli Studi di Napoli Federico II, p.le Tecchio 80, 80125 Napoli, Italy
[b] Dipartimento di Ingegneria, Università degli Studi del Sannio, corso Garibaldi 107, Palazzo dell'Aquila Bosco Lucarelli, 82100 Benevento, Italy

ARTICLE INFO

Article history:
Received 25 November 2008
Accepted 16 April 2009
Available online 6 June 2009

Keywords:
Carbon dioxide
Heat transfer coefficient
Flow regime
Boiling
Evaporator

ABSTRACT

Carbon dioxide is gaining renewed interest as an environmentally safe refrigerant. In order to improve the energy efficiency of R744 systems, an accurate knowledge of heat transfer coefficients is fundamental.

In this paper experimental heat transfer coefficients during flow boiling of R744 in a smooth, horizontal, circular, 6.00 mm inner diameter tube are presented. We obtained 217 experimental points in 18 operating conditions commonly encountered in dry-expansion evaporators investigating the effect of the mass flux within the range from 200 to 349 kg/m^2 s, the saturation temperature within the range from −7.8 to 5.8 °C, the heat flux within the range from 10.0 to 20.6 kW/m^2 and the vapor quality within the range from 0.02 to 0.98.

An interpretation of the experimental trends based on the local circumferential distribution of heat transfer coefficients, the flow regimes and the thermophysical properties is proposed.

Besides the measured data are compared with those predicted by the Cheng et al. [L. Cheng, G. Ribatski, J.R. Thome, New prediction methods for CO_2 evaporation inside tubes: Part II – An updated general flow boiling heat transfer model based on flow patterns, International Journal of Heat and Mass Transfer 51 (2008) 125–135] and Yoon et al. [R. Yun, Y. Kim, M.S. Kim, Y. Choi, Boiling heat transfer and dryout phenomenon of CO_2 in a horizontal smooth tube, International Journal of Heat and Mass Transfer 46 (2003) 2353–2361] correlations to determine the best predictive method for the tested operating conditions.

1. Introduction

In the field of refrigeration *HCFC*s have been scheduled for phase-out [1]. The *HFC*s, that were once expected to be acceptable permanent replacement fluids due to their null contribution to ozone depletion, are now on the list of regulated substances due to their impact on climate change and there is growing concern about future use [2]. The focus on greenhouse effect of fluorinated compounds has led to a proposed gradual phase-out of refrigerants with *GWP* > 150 (i.e. the most part of *HFC*s) in mobile air conditioning in EU, starting from 2008 [3] and some countries are moving unilaterally toward restrictions on and even bans of some *HFC* uses [4]. In this situation the industry is looking for completely different long-term solutions. Over of continuing the search for new chemicals, there is an increasing interest in technology based on ecologically safe natural refrigerants. Among these, carbon dioxide is seen today as one of the most promising refrigerants and great interest is raising in industrial and scientific fields [5–7], because it is an ozone friendly, with negligible *GWP*, non toxic and non flammable fluid.

On the other side carbon dioxide vapor pressure is much higher than *HCFC*s and *HFC*s. As a consequence it is not possible to consider carbon dioxide as a drop-in refrigerant of conventional refrigerants: its use implicates the necessity to redesign completely the vapor compression plants and the constraints arising from the very high pressure levels lead to expensive CO_2 systems and make it hard to manufacture the components. Besides it can be noticed that the single stage vapor compression plants that use R744 as working fluid operate usually on a transcritical cycle. This leads to CO_2 does not compare favourably against traditional refrigerants, as far as energy efficiency is concerned when theoretical cycle analyses are carried out. Taking into account that the climate change is influenced not only by the refrigerant leakages, but also by energy consumption during the lifetime of refrigerating equipment, the essential option to lower the environmental impact is to improve the energy efficiency of the R744 systems. To maximize the performances of a vapor compression plant, a proper design of each component is necessary. Among the components which influence the cycle efficiency, the evaporator is of particular importance. To optimize the design of evaporators, the accurate knowledge of heat transfer coefficients is fundamental. Indeed, it can reduce costs by avoiding underdesign and, therefore, it is a prerequisite to increase the plant performance through the correct sizing.

* Corresponding author. Tel.: +39 0 81 7682303; fax: +39 0 81 2390364.
E-mail address: antonio.rosato@unina.it (A. Rosato).

0017-9310/$ - see front matter © 2009 Elsevier Ltd. All rights reserved.
doi:10.1016/j.ijheatmasstransfer.2009.04.004

Nomenclature

Latin letters

A_{VD}	dimensionless cross-sectional area occupied by vapor phase
Bo	bond number
d	diameter (m)
d_d	bubble departure diameter (m)
f	frequency of bubble release (Hz)
G	refrigerant mass flux (kg/m^2 s)
G_{wavy}	wavy flow transition mass velocity (kg/m^2 s)
G_{strat}	stratified flow transition mass velocity (kg/m^2 s)
GWP	global warming potential
h	local heat transfer coefficient (W/m^2 K)
h_{LD}	dimensionless vertical height of liquid
HFC	HydroFluoroCarbons
HCFC	HydroChloroFluoroCarbons
Fr	Froude number
i	specific enthalpy (kJ/kg)
i_{lv}	latent heat of vaporization (kJ/kg)
Ja	Jakob number
k	thermal conductivity (W/m K)
L	length (m)
$\dot{m}$	mass flow rate (kg/s)
N	number of points
Nu	Nusselt number
ODP	ozone depleting potential
p	pressure (bar)
Pr	Prandtl number;
q	heat flux (W/m^2)
$\dot{Q}$	power (W)
r	radius (m)
R	electrical resistance (Ω)
sd	standard deviation (%)
t	temperature (°C)
V	voltage (V)
We	Weber number
x	vapor quality
x_{di}	dryout inception quality

Greeks

α	cross-sectional vapor void fraction
β	contact angle (rad.)
δ_l	liquid film thickness (m)
Δ	difference
ε_n	error (%)
$\bar{\varepsilon}$	mean error (%)
$\lvert\bar{\varepsilon}\rvert$	mean absolute error (%)
λ	number of experimental points predicted within ±30%
μ	dynamic viscosity (μPa s)
ρ	density (kg/m^3)
σ	surface tension (N/m)

Subscripts

A	annular
ATS	adiabatic test section
cr	critical
DTS	diabatic test section
exp	experimental
I	intermittent flow
i	inner
in	inlet
l	liquid
M	referred to measurement section M
nb	nucleate boiling
o	outer
PH	preheater
pred	predicted
r	reduced
sat	saturation
SUP	fully suppression of nucleate boiling
v	vapor
w	wall

In literature several experimental studies on CO_2 two-phase heat transfer during flow boiling in horizontal circular macrochannels are available. Thome and Ribatski [8] have recently given a review of flow boiling heat transfer and two-phase flow of CO_2 in macrochannels. The experiments analyzed in this work have been performed for saturation temperatures from −25 to 20 °C, heat flux from 3 to 30 kW/m^2 and mass flux from 85 to 1440 kg/m^2 s. The test sections adopted were smooth or micro-fin tubes with an inner diameter from 4 to 10.06 mm heated by Joule effect or by a secondary fluid. In comparison to the conventional refrigerants, in these experimental studies the authors observed that:

- CO_2 flow regimes compared with the flow pattern maps that were developed for other fluids denotes significant deviations (many works underlined that dryout may occur at much lower vapor quality, particularly at high mass flux and evaporating temperature);
- CO_2 nucleate boiling contribution seems to be predominant;
- CO_2 heat transfer coefficients are higher;
- the available heat transfer prediction methods, developed using experimental databases containing mainly low and medium pressure refrigerants, generally underpredict the experimental data of CO_2.

These differences can be explained taking into account that, compared to the traditional fluids, carbon dioxide has thermodynamic and transport properties much different (higher reduced pressure, vapor density and thermal conductivity and lower surface tension). Nevertheless, more accurate local heat transfer data are still needed. In fact in literature some works presented experimental results that are quite different from those obtained in comparable operating conditions [9–13]. Besides it seems that the interpretation of the trends of experimental points is still opened. In particular, the influence of mass flux, evaporating temperature, heat flux and vapor quality on the heat transfer coefficients is not completely cleared and some contradictions appears in the data as it is evident comparing some works [9–17].

For the reasons specified above, the local heat transfer coefficient of R744 during flow boiling in a smooth, horizontal, circular, stainless steel tube with an inner diameter of 6.00 mm are experimentally evaluated. The tests were carried out by means of a new experimental apparatus developed for accurate carbon dioxide measurements. We obtained 217 experimental points in 18 operating conditions commonly encountered in dry-expansion evaporators varying the refrigerant mass flux within the range from 200 to 349 kg/m^2 s, the evaporating pressure within the range from 28.2 to 40.5 bar (saturation temperature within the range from −7.8 to 5.8 °C), the heat flux within the range from 10.0 to 20.6 kW/m^2 and the vapor quality within the range from 0.02 to 0.98. An interpretation of the experimental trends based on the local circumferential distribution of heat transfer coefficients, the flow regimes and the thermophysical properties is proposed.

2. Experimental plant

A schematic view of the plant is shown in Fig. 1. The experimental apparatus allows to measure simultaneously the local heat transfer coefficients and pressure gradients during flow boiling. At this scope two test sections were installed: the first one is diabatic, while the second one is adiabatic The refrigerant loop consists of a magnetic gear pump, a preheater, an adiabatic and a diabatic test section, a shell-and-tube heat exchanger, a brazed plate heat exchanger and a tube-in-tube subcooler.

The magnetic gear pump drives the fluid coming from the liquid reservoir. The refrigerant mass flux can be modified varying the electric motor speed by an inverter. The refrigerant, in sub-cooled conditions, passes first through the preheater where heat is supplied to the fluid by four fibreglass heating tapes (each one has a nominal power of 830 W at 240 V (AC)); changing the voltage it is possible to modify the thermal power and to obtain the desired quality at the diabatic test section inlet. After the preheater, the fluid flows through the diabatic test section. Upstream the latter, a straight tube of 60.0 cm length allows the fully development of the flow.

The diabatic test section is a smooth, horizontal, circular, stainless steel (type 304) tube with an inner radius of 3.00 ± 0.05 mm, a outer radius of 4.00 ± 0.05 mm and a length of 1200.0 ± 0.5 mm at 20 °C and 1.0 bar. The thermal power is provided to the fluid by Joule effect by a feed current device.

After the evaporation, the refrigerant passes the adiabatic test section and then condenses in a shell-and-tube heat exchanger and in a brazed plate heat exchanger. Before returning to the pump, the refrigerant is sub-cooled in a tube-in-tube heat exchanger. The coolant is an auxiliary fluid (TEMPER) contained in a storage tank of 200 dm^3. It can be chilled down to −30 °C by a R404A auxiliary refrigerating plant and it is circulated by a magnetic gear pump connected to an inverter. By adjusting the refrigerant charge, the TEMPER inlet temperature and mass flow rate, it is possible to modify and hold constant the refrigerant evaporating pressure in the test section. To avoid heat gains, heavy insulation was provided by an elastomeric insulator (k = 0.035 W/m K at 0.0 °C) for the two test sections, shell-and-tube heat exchanger, the tube-in-tube subcooler, the liquid reservoir, the tubes and the tube fittings; by a 32 mm layer of cellular insulator (k = 0.040 W/m K at 40 °C) for the plate heat exchanger and by 5 cm layer of rock wool insulator (k = 0.075 W/m K at 300 °C) for the preheater.

3. Data acquisition, data reduction and uncertainty analysis

To run the calculations of the local heat transfer coefficient and vapor quality the following assumptions are made:

- steady-state conditions;
- the refrigerating loop is adiabatic to the surroundings;
- the tube of the diabatic test section is homogeneous and isotropic, so that the heat generation inside the tube due to the Joule effect can be safely considered uniform;
- there are no electric leakages from the diabatic test section to the remaining part of the loop, since dielectric fittings are used at the test section inlet and outlet;
- the effect of axial conduction into the diabatic test section to the tube wall temperature measurements is negligible;
- heating power of the preheater and of the diabatic test section is completely transferred to the fluid;
- the heat flux at the inner wall of the diabatic test section is uniform.

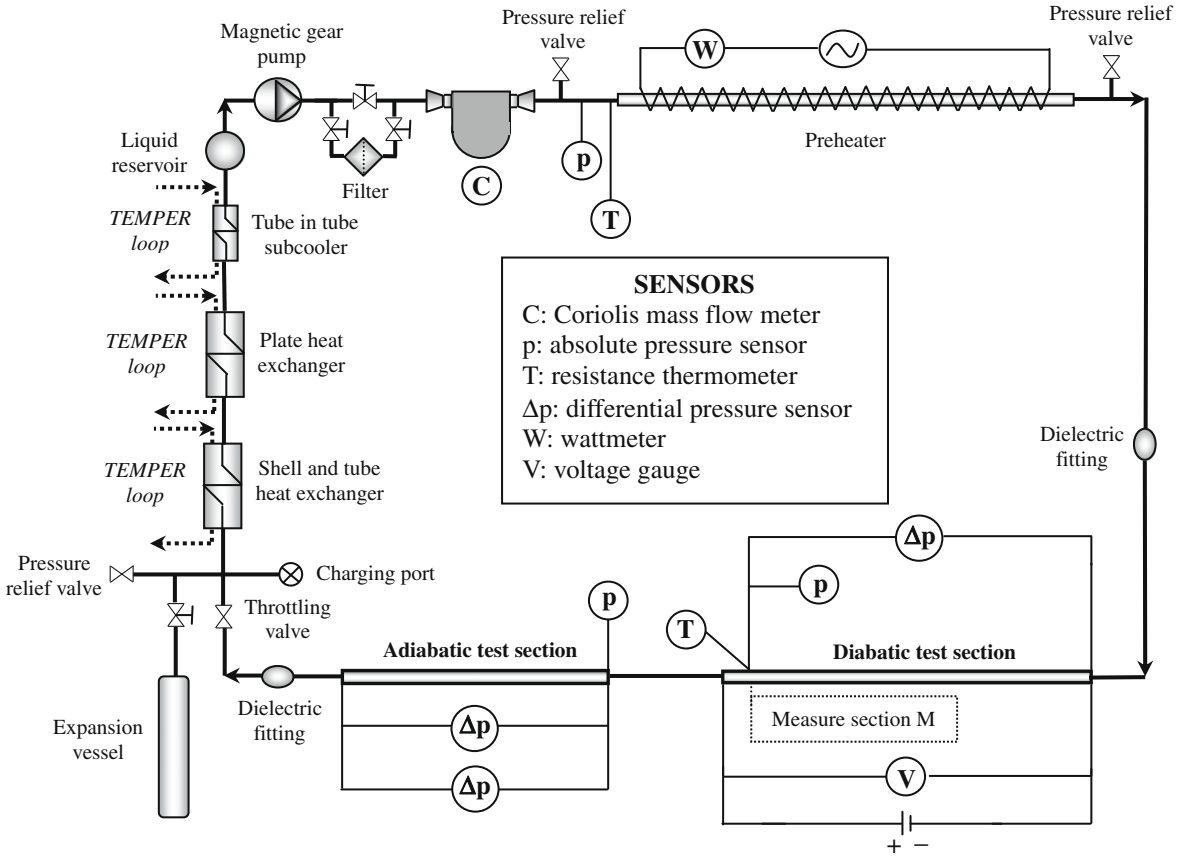

Fig. 1. Experimental apparatus scheme.

The local heat transfer coefficient is measured in the section M, far away 200.0 ± 0.05 mm from the exit of the diabatic, by the Newton equation:

$$h = \frac{\dot{Q}_{DTS}}{2\pi r_{i,DTS} L_{DTS}(t_{w,i} - t_{sat})} = \frac{q}{(t_{w,i} - t_{sat})} \quad (1)$$

Heating power provided to the fluid is calculated measuring the voltage V_{DTS} between the inlet and the exit of the tube by an electrical voltage transducer; the electrical resistance of tube R_{DTS} from the calibration certificate is 0.037121 Ω ± 0.056 mΩ at −4.90 °C and 0.039159 ± 0.059 mΩ at 35.00 °C. t_{sat} is obtained from the absolute pressure p_{sat}, which is measured at section M by means of a piezoelectric absolute pressure transducer. $t_{w,i}$ is calculated from the measured outside wall temperature $t_{w,o}$ by applying the one-dimensional, radial, steady-state heat conduction equation for a hollow cylinder with a uniform heat generation. $t_{w,o}$ is measured with four four-wire Pt100 resistance thermometers mounted on the top, the bottom, the left and the right sides of the tube in order to taking into account the liquid and vapor spatial distribution. Four values of $t_{w,i}$ and, therefore, four local heat transfer coefficients h_{top}, h_{bottom}, h_{left}, h_{right} are obtained.

At the section M, the vapor quality is obtained from the local saturation pressure p_{sat} and the specific enthalpy i_M; the latter is calculated by an energy balance between the inlet of the preheater and the section M:

$$i_M = i_{in,PH} + \frac{\dot{Q}_{PH}}{\dot{m}} + \frac{\dot{Q}_{in,DTS\text{-}M}}{\dot{m}} \quad (2)$$

The specific enthalpy at the inlet of the preheater is evaluated from the absolute pressure $p_{in,PH}$ and the temperature $t_{in,PH}$. The heating power provided to the refrigerant in the preheater is measured with a wattmeter, while the heating power supplied to the fluid between the diabatic test section inlet and the measurement section is determined as $R_{in,DTS\text{-}M}\frac{V_{DTS}^2}{R_{DTS}^2}$, where $R_{in,DTS\text{-}M}$ is the electrical resistance of the considered part of the heated channel (0.030209 Ω ± 0.045 mΩ at −4.90 °C and 0.032168 ± 0.045 mΩ at 34.60 °C). The refrigerant mass flow rate $\dot{m}$ is measured by a Coriolis effect mass flow meter working in the liquid line.

All the thermodynamic properties are calculated by the software REFPROP [18].

Table 1 summarizes the measurement characteristics of the plant instrumentation.

The uncertainties for the local heat transfer coefficient and for the vapor quality at section M were calculated according to the single-sample uncertainty analysis suggested by Moffat [19].

For data acquisition and storage, a personal computer connected with a 16 bit resolution data acquisition system, provided with a software for monitoring experimental values, is used. The logging of signals from all the sensors is performed on all the channels for 100 s with 1.0 Hz acquisition frequency and the average values of each channel are stored. If the deviation of each value from its average value is lower than a fixed quantity, steady-state conditions are assumed. The plotted values of heat transfer coefficient h_M are obtained as follows:

$$h_M = \sum_{n=1}^{100} h_{M,i} = \sum_{n=1}^{100} \left(\frac{h_{top} + h_{bottom} + h_{left} + h_{right}}{4} \right)_n \quad (3)$$

4. Preliminary tests

The reliability of the measurements was verified through three different checks: (i) single-phase R134a heat transfer coefficient measurements, (ii) single-phase energy balance and (iii) repeatability of the measurements.

Table 1
Measurement equipment.

Measurement	Device	Calibration range	Uncertainty
Δp_{ATS}	Piezoelectric differential pressure transducer	0 ÷ 10 kPa	±0.075% of full scale
	Piezoelectric differential pressure transducer	0 ÷ 100 kPa	±0.075% of full scale
$p_{in,ATS}$	Piezoelectric absolute pressure transducer	0 ÷ 50 bar	±0.1% of full scale
$t_{in,PH}$	Probe resistance thermometer Pt100	−50 ÷ 100 °C	±0.1 °C
$p_{in,PH}$	Piezoelectric absolute pressure transducer	0 ÷ 50 bar	±0.1% of range
$t_{w,o}$	Resistance thermometer Pt100	−50 ÷ 100 °C	±0.03 °C
Q_{PH}	Wattmeter	0 ÷ 3600 W	±0.2% of reading + 0.02% of full scale
V_{DTS}	Electronic voltage transducer	0 ÷ 10 V	±0.19% of reading + 0.01% of full scale
m	Coriolis mass flow meter	0 ÷ 1.8 kg s^{-1}	±0.05% of reading
p_{sat}	Piezoelectric absolute pressure transducer	0 ÷ 50 bar	± 0.1% of full scale

Twenty experiments were carried out with mass velocities ranging from 701 to 1005 kg/m² s covering a range of Reynolds numbers from 13,251 up to 22,066 (turbulent flow).

The R134a single-phase Nusselt number was compared to the well-known correlations of Dittus–Boelter [20] and Gnielinski [21]. The comparison has been characterized by the following parameters:

$$\varepsilon_n = \left(\frac{h_{pred,n} - h_{exp,n}}{h_{exp,n}} \right) \quad (4)$$

$$\bar{\varepsilon} = \frac{1}{N} \sum_{n=1}^{N} \varepsilon_n \quad (5)$$

$$|\bar{\varepsilon}| = \frac{1}{N} \sum_{n=1}^{N} |\varepsilon_n| \quad (6)$$

$$sd = \sqrt{\frac{1}{N} \sum_{n=1}^{N} (\varepsilon_n - \bar{\varepsilon})^2} \quad (7)$$

Fig. 2 shows a very good agreement between the experimental and predicted values. In fact Dittus–Boelter correlation [20] predicts the experimental Nusselt number with a mean error of −3.6%, an absolute mean error of 1.6% and a standard deviation equal to 1.9%, while for Gnielinski correlation [21] it results $\bar{\varepsilon} = 1.2\%$, $|\bar{\varepsilon}| = 1.1\%$ and sd = 2.2%. Dittus–Boelter correlation [20] is able to predict the 100% of data within ±7%, while Gnielinski correlation [21] predicts all points within ±4%.

Concerning the energy balance, the absolute mean error was always less than 3.5%, which is a good result for this type of experiments.

The measurement repeatability was investigated in a fixed operating condition ($G \approx 300$ kg/m² s, $p_{sat} \approx 3.5$ bar, q = 10 kW/m²) four times: Fig. 3 shows the agreement of the local heat transfer data. The performed preliminary tests showed an instrument calibration and overall system performance consistent with the desired accuracy.

5. Experimental results and flow regime analysis

The operating conditions investigated in this study are summarized in Table 2: in this table, the refrigerant mass flux, the evaporating pressure (and the corresponding saturation temperature),

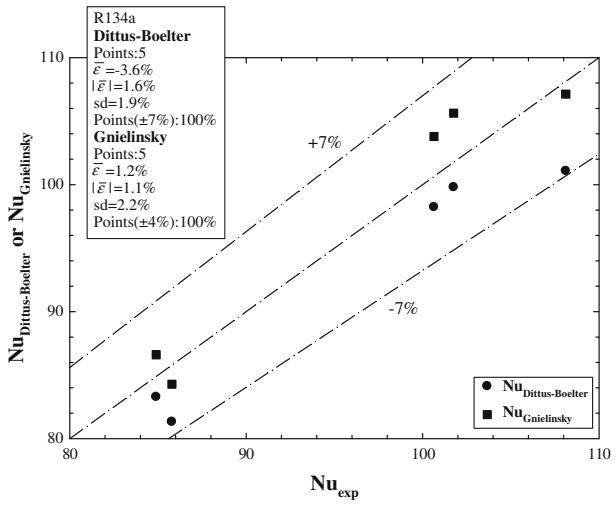

Fig. 2. Comparison of single-phase R134a heat transfer coefficient measurements to predictions by the correlations of Dittus–Boelter [20] and Gnielinski [21].

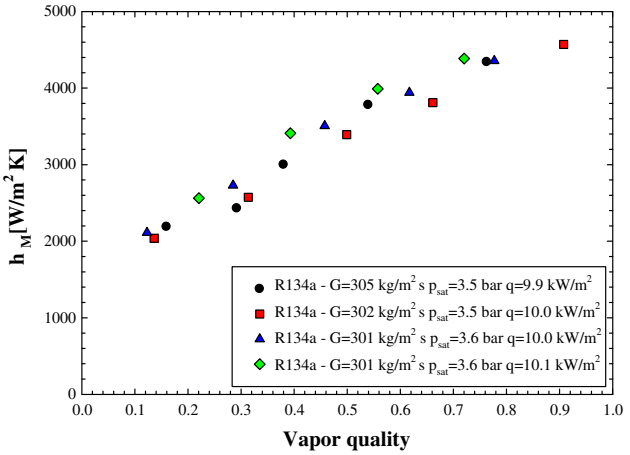

Fig. 3. Local heat transfer coefficient of R134a as a function of vapor quality: a fixed operating condition ($G \approx 300$ kg/m^2 s, $p_{sat} \approx 3.5$ bar, $q \approx 10.0$ kW/m^2) investigated four times.

Table 2
The operating conditions.

G (kg/m^2 s)	p_{sat} (bar)	t_{sat} (°C)	q (kW/m^2)	Δx_{exp}
200	28.2	−7.8	10.1	0.12 ÷ 0.98
200	39.7	5.0	20.3	0.27 ÷ 0.96
201	39.7	5.0	15.2	0.41 ÷ 0.88
202	38.9	4.2	10.1	0.13 ÷ 0.96
203	32.0	−3.2	10.1	0.13 ÷ 0.94
250	28.2	−7.8	10.1	0.09 ÷ 0.82
251	32.0	−3.2	10.1	0.09 ÷ 0.75
252	40.4	5.7	10.2	0.07 ÷ 0.93
297	32.1	−3.1	10.1	0.07 ÷ 0.88
300	39.7	5.0	20.2	0.17 ÷ 0.85
300	40.5	5.8	10.3	0.09 ÷ 0.85
301	28.2	−7.8	10.1	0.07 ÷ 0.97
302	39.7	5.0	15.5	0.25 ÷ 0.86
348	28.3	−7.7	20.0	0.18 ÷ 0.78
348	39.7	5.0	10.0	0.02 ÷ 0.93
348	39.7	5.0	20.6	0.30 ÷ 0.88
349	28.2	−7.8	10.1	0.10 ÷ 0.76
349	32.0	−3.2	10.1	0.05 ÷ 0.78

the heat flux and the vapor quality range are specified for each test. The relative measurement uncertainty in the evaluation of the local heat transfer coefficient ranges between 3.4% and 6.5%, while the uncertainty in the evaluation of the vapor quality at the measurement section M is always lower than 3.1%.

Fig. 4 depicts the local heat transfer coefficient of R744 as a function of vapor quality at varying refrigerant mass flux from about 200 to about 350 kg/m^2 s for $t_{sat} = -7.8$ °C, $t_{sat} \approx -3$ °C and $t_{sat} \approx 5$ °C. For all plots it results $q \approx 10$ kW/m^2. Very similar trends have been observed experimentally by Yun et al. [11] and Oh et al. [16]: they explain their experimental results in terms of partial dryout of liquid film at very low vapor quality (0.3 ÷ 0.4) and dominance of nucleate boiling. Taking into account that the heat transfer process depends on the liquid and vapor phase distributions, an accurate analysis of the flow regimes corresponding to the experimental points is necessary to understand the experimental values and trends. At this scope, in Fig. 5 we reported the heat transfer coefficient at the bottom, right, top and left side of the measurement section as a function of vapor quality at a saturation temperature of about −3 °C for (a) $G \approx 200$ kg/m^2 s, (b) $G \approx 250$ kg/m^2 s, (c) $G \approx 300$ kg/m^2 s and (d) $G \approx 350$ kg/m^2 s. The tests carried out at $t_{sat} = -7.8$ °C and $t_{sat} \approx 5$ °C showed a variation of the heat transfer coefficient around the tube periphery very similar to that observed for $t_{sat} \approx -3$ °C. The experimental results show a considerable variation of the heat transfer coefficient around the periphery of the tube at low vapor qualities (up to around 25%), with the top of the tube having the highest heat transfer coefficient for all the refrigerant mass fluxes tested. At higher vapor qualities, the heat transfer coefficient at the top being lower than the heat transfer coefficient at the bottom for $G \approx 200$ kg/m^2 s (Fig. 5a), while there are no obvious differences between the top and the bottom for $G \approx 250$ kg/m^2 s and $G \approx 300$ kg/m^2 s (Fig. 5b and c). For $G \approx 350$ kg/m^2 s (Fig. 5d) the heat transfer coefficient at the top becomes always somewhat larger than that at the bottom.

The important differences between the top and bottom of the tube shown at low vapor qualities can be explained analyzing the flow regimes. One of the most widely used flow pattern transition maps developed specifically for carbon dioxide is that due to Cheng et al. [22,23] and this map has been selected for comparison with our data. The dryout inception vapor quality x_{di} predicted by the flow pattern map of Cheng et al. [22,23] for $G = 350$ kg/m^2 s is reported in Table 3: it is possible to observe that, at the evaporating temperatures considered in this study, for carbon dioxide x_{di} (even if lower than that calculated for R22 as suggested by [24,25]) is always higher than 0.90. At decreasing mass flux, x_{di} increases: therefore it is reasonable to suppose that partial dryout cannot occur for the operating conditions tested in this work at low vapor quality. Concerning with the flow regime transitions that happen for low vapor qualities, this map distinguishes between slug zone, slug/stratified-wavy zone and intermittent zone (only for very low refrigerant mass flux the stratified flow regime can exists). The intermittent to annular flow transition boundary is calculated with the following relation:

$$x_{I-A} = \left[1.8^{\frac{1}{0.875}}\left(\frac{\rho_v}{\rho_l}\right)^{-\frac{1}{1.75}}\left(\frac{\mu_l}{\mu_v}\right)^{-\frac{1}{7}} + 1\right]^{-1} \tag{8}$$

Eq. (8) provides also the vapor quality transition from the slug/stratified-wavy zone to the stratified-wavy zone. From Eq. (8) it can be observed that x_{I-A} is independent from refrigerant mass flux and it is only a function of the saturation temperature: for $t_{sat} = -8$ °C it results $x_{I-A} = 0.14$, while for $t_{sat} = 5$ °C x_{I-A} is equal to 0.17. In the flow pattern map of Cheng et al. [22,23] the transition boundary from the stratified-wavy zone to intermittent or annular flow region is calculated with the following relation:

$$G_{wavy} = \left\{\frac{16A_{VD}^3 g d_i \rho_l \rho_v}{x^2\pi^2[1-(2h_{LD}-1)^2]^{\frac{1}{2}}}\left[\frac{\pi^2}{25h_{LD}^2}\left(\frac{Fr_l}{We_l}\right)+1\right]\right\}^{\frac{1}{2}} + 50 \tag{9}$$

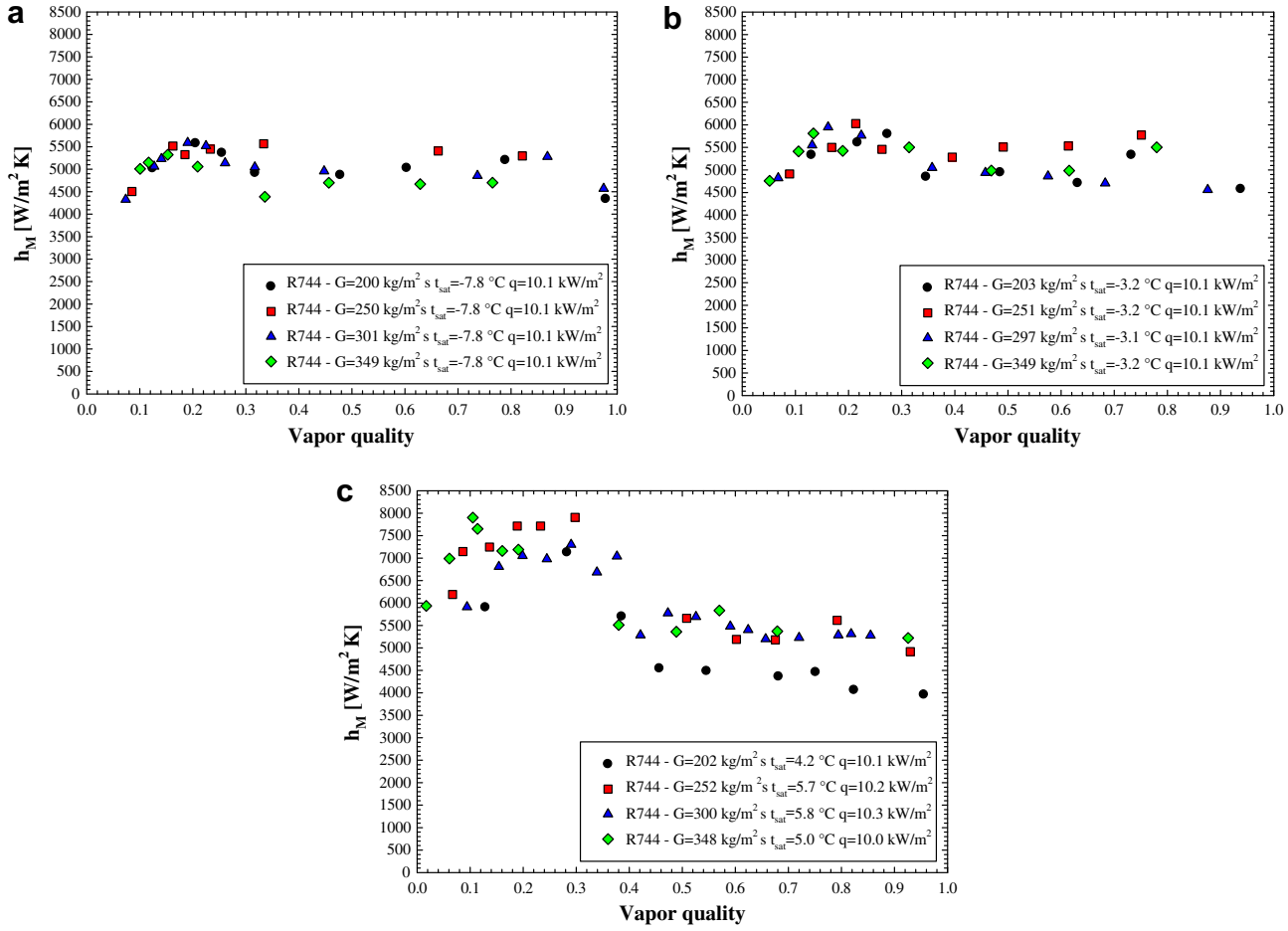

Fig. 4. Local heat transfer coefficients of R744 as a function of vapor quality at varying refrigerant mass flux from about 200 to about 350 kg/m^2 s for (a) $t_{sat} = -7.8$ °C, (b) $t_{sat} \approx -3$ °C and (c) $t_{sat} \approx 5$ °C.

with

$$A_{VD} = \frac{A\alpha}{d_i^2}, \quad h_{LD} = 0.5\left[1 - \cos\left(\frac{2\pi - \theta_{strat}}{2}\right)\right],$$
$$Fr_l = \frac{G^2}{\rho_l^2 g d_i}, \quad We_l = \frac{G^2 d_i}{\rho_l \sigma} \tag{10}$$

The cross-sectional void fraction is determined from the Steiner [26] version of the Rouhani–Axelsson drift flux model for horizontal tubes, while the stratified angle is calculated with the equation proposed by Biberg [27]. When $G > G_{wavy}$ and $x < x_{I-A}$ the flow regime is intermittent, while for $G > G_{wavy}$ and $x \geqslant x_{I-A}$ the flow regime is annular. For $G < G_{wavy}$, the flow pattern map of Cheng et al. [22,23] predicts the stratified-wavy flow subdividing the stratified-wavy flow region into three zones:

- $G > G_{wavy}(x_{I-A})$ and $x < x_{I-A}$ give the slug flow zone;
- $G_{strat} < G < G_{wavy}(x_{I-A})$ and $x < x_{I-A}$ give the slug/stratified-wavy zone;
- $G_{strat} < G < G_{wavy}(x_{I-A})$ and $x \geqslant x_{I-A}$ give the stratified-wavy zone.

From Eq. (8) it can be obtained that, for $G = 200$ kg/m^2 s, $G_{wavy}(x_{I-A}) = 216$ kg/m^2 s for $t_{sat} = -8$ °C, $G_{wavy}(x_{I-A}) = 206$ kg/m^2 s for $t_{sat} = -3$ °C and $G_{wavy}(x_{I-A}) = 190$ kg/m^2 s for $t_{sat} = 5$ °C. For $G = 350$ kg/m^2 s, $G_{wavy}(x_{I-A})$ is equal to 232 kg/m^2 s for $t_{sat} = -8$ °C, 220 kg/m^2 s for $t_{sat} = -3$ °C and 203 kg/m^2 s for $t_{sat} = 5$ °C.

Therefore we can reasonably assume that, for the operating conditions investigated in this work, the experimental points corresponding to low vapor qualities (up to around 25%) are in the slug flow regime. Mainly for low vapor qualities the nucleate boiling contribution is dominant: Sun et al. [28] showed that the contribution to the overall coefficient of the liquid slug region is small (most of the heat transfer occurring in the film region (namely the region between the liquid slugs)) and that the nucleate boiling coefficient in liquid film at the top of the film region is more than that in the liquid film at the bottom of the film region because the faster moving, more turbulent, bottom liquid film gives a greater nucleate boiling suppression. These results can explain the experimental trends observed in Fig. 5 for low vapor qualities where the top of the tube have a heat transfer coefficient higher than that pertaining to the bottom.

At higher vapor qualities, for $G = 203$ kg/m^2 s, the heat transfer coefficient at the top of the tube become lower than that corresponding to the bottom, right and left sides of the measurement section; this is probably due to the change from slug to stratified-wavy flow regime. In the latter the vapor goes to the top and the liquid to the bottom of the tube with waves at the interface that travel in the direction of the flow. The amplitude of the waves is notable, but their crests do not reach the top of the tube. As a consequence the wall temperature at the top of the tube rises, which leads to the decrease in the corresponding heat transfer coefficient (Fig. 5a). At increasing the refrigerant mass flux ($G = 251$ kg/m^2 s and $G = 297$ kg/m^2 s), there are no relevant differences in the heat transfer coefficient around the periphery of the tube for a vapor quality higher than around 0.3 (Fig. 5b and c). This is probably the consequence of the transition from slug flow to

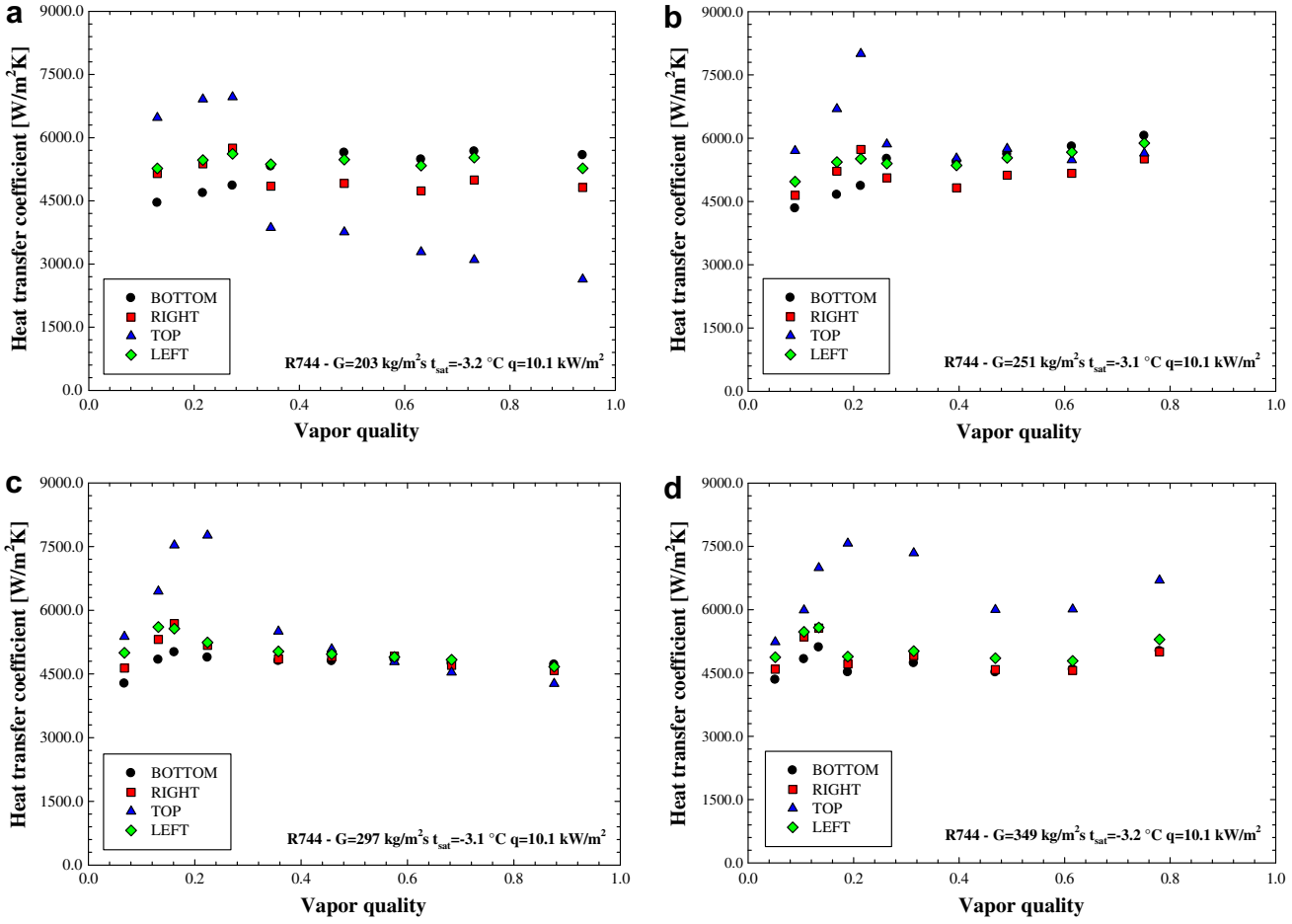

Fig. 5. Variation of circumferential heat transfer coefficient with respect to vapor quality for $t_{sat} \approx -3$ °C, $q = 10.1$ kW/m^2 and (a) $G \approx 200$ kg/m^2 s, (b) $G \approx 250$ kg/m^2 s, (c) $G \approx 300$ kg/m^2 s and (d) $G \approx 350$ kg/m^2 s.

annular flow with an almost uniform liquid film thickness around the periphery of the tube. The flow pattern map of Cheng et al [22,23] confirms this interpretation: in fact, in the considered experiments, it results $x > x_{I-A}$ and $G > G_{wavy}(x_{I-A})$. At increasing refrigerant mass flux, the liquid film at the top of the tube, due to the gravity force, becomes thinner. In fact, at increasing the mass flow rate, the dryout inception vapor quality predicted by Cheng et al. [22,23] becomes lower; Mori et al. [29] and Wojtan et al. [24,25] also verified experimentally that the dryout inception at the top of the tube appears at lower vapor qualities as the mass velocity increases. Therefore for $G \approx 350$ kg/m^2 s (Fig. 5d) the flow regime is probably still annular, but the liquid film is not still uniform around the periphery of the tube. In particular the thermal resistance of the liquid film at the top of the tube becomes lower: as a consequence the heat transfer coefficient at the top of the tube results somewhat higher than that pertaining to the bottom, the right and left sides of the section M for vapor qualities higher than around 0.3.

5.1. Influence of vapor quality

Generally, in case of conventional refrigerants, it is known that the local heat transfer coefficient increases with the vapor quality once the annular flow regime is reached. No similar results have been observed in our experiments. In fact in our tests at low evaporating temperatures the CO_2 heat transfer coefficient is nearly independent of vapor quality. This can be explained taking into account that the influence of convective boiling for carbon dioxide is reduced because of high vapor to liquid densities ratio: therefore, the fluid is not accelerated so much by evaporation. From Table 3 it can be observed that, for all values of saturation temperatures considered, carbon dioxide has a ratio ρ_v/ρ_l about six times larger than R22. Besides, in the annular flow region, the convective boiling contribution is proportional to the ratio between the liquid thermal conductivity and the liquid film thickness ratio. Evaluating δ_l as suggested by Kattan et al. [30], it can be observed that carbon dioxide has a ratio k_l/δ_l around 1.5 times lower than R22 for the evaporating temperatures tested in this work.

The particular dependence of the heat transfer coefficient from the vapor quality can be explained also taking into account that carbon dioxide reveals stronger nucleate boiling heat transfer characteristics due to its physical properties. In fact, it is known that, for a given liquid superheat Δt, the critical bubble radius r_{cr} for a pure substance can be calculated as follows [31]:

$$r_{cr} = \frac{2 t_{sat} \sigma}{i_{lv} \rho_v \Delta t} \tag{11}$$

Bubbles that are smaller in radius than r_{cr} will collapse spontaneously and bubbles that are bigger in radius than r_{cr} will grow: hence, a lower value of r_{cr} implies a stronger nucleate boiling contribution, which may positively affect heat transfer, mainly at medium-low vapor quality. From Table 3 it can be noticed that, for $\Delta t = 1$ K, the CO_2 critical bubble radius is about fifteen times smaller than that pertaining to R22. This is due to the fact that, compared to R22, R744 has a lower surface tension and a latent heat of vaporization and vapor density higher.

Table 3
Thermophysical properties of R744 and R22.

		R744	R22
t_{sat} = −8 °C	x_{di}[a]	0.941	0.947
	ρ_v/ρ_l	0.078	0.013
	r_{cr} (μm)[b]	0.168	1.976
	f (Hz)[c]	94.9	88.0
	x_{SUP}[d]	0.986	0.870
	$h_{nb,COOPER}$ (W/m² K)[e]	5690.9	1955.4
	$h_{nb,JUNG\ and\ RADERMACHER}$ (W/m² K)[e]	4157.6	1455.6
	$h_{nb,MOSTINSKI}$ (W/m² K)[e]	3411.9	1260.0
t_{sat} = −3 °C	x_{di}[a]	0.939	0.949
	ρ_v/ρ_l	0.094	0.015
	r_{cr} (μm)[b]	0.130	1.639
	f (Hz)[c]	97.1	89.1
	x_{SUP}[d]	0.989	0.895
	$h_{nb,COOPER}$ (W/m² K)[e]	6295.2	2072.2
	$h_{nb,JUNG\ and\ RADERMACHER}$ (W/m² K)[e]	4616.8	1572.5
	$h_{nb,MOSTINSKI}$ (W/m² K)[e]	3734.6	1330.7
t_{sat} = 5 °C	x_{di}[a]	0.934	0.951
	ρ_v/ρ_l	0.128	0.020
	r_{cr} (μm)[b]	0.082	1.222
	f (Hz)[c]	101.5	90.9
	x_{SUP}[d]	0.993	0.926
	$h_{nb,COOPER}$ (W/m² K)[e]	7581.9	2275.4
	$h_{nb,JUNG\ and\ RADERMACHER}$ (W/m² K)[e]	5604.8	1773.8
	$h_{nb,MOSTINSKI}$ (W/m² K)[e]	4347.1	1457.2

[a] G = 350 kg/m² s, q = 10 kW/m².
[b] Δt = 1 K.
[c] $t_{w,i} - t_{sat}$ = 1 K.
[d] G = 200 kg/m² s, q = 10 kW/m².
[e] q = 10 kW/m².

The nucleate contribution can be characterized not only by the critical bubble radius, but it also depends on the frequency of bubble release f. The latter is a function of the bubble departure diameter d_d, i.e. of the specific bubble size at which, for a given cavity, bubble release can occurs. Zuber [32] suggested the following relation to evaluate f:

$$f = \frac{0.59}{d_d}\left[\frac{\sigma g(\rho_l - \rho_v)}{\rho_l^2}\right]^{\frac{1}{4}} \tag{12}$$

Jensen and Memmel [33] compared the available correlations able to predict the bubble departure diameter against available bubble departure diameter data: the correlation of Kutateladze and Gogonin [34] was found the best overall fit to the data examined. Jensen and Memmel [33] also proposed an improved version of Kutateladze and Gogonin correlation [34]:

$$Bo^{\frac{1}{2}} = 0.91(1.8 + 10^5 K_l)^{\frac{2}{3}} \tag{13}$$

where Bo is the Bond number:

$$Bo = \frac{g(\rho_l - \rho_v)d_d^2}{\sigma} \tag{14}$$

and K_l is given by the equation:

$$K_l = \left(\frac{Ja}{Pr_l}\right)\left\{\left[\frac{g\rho_l(\rho_l - \rho_v)}{\mu_l^2}\right]\left[\frac{\sigma}{g(\rho_l - \rho_v)}\right]^{\frac{3}{2}}\right\}^{-1} \tag{15}$$

with the Jakob number Ja defined as follows:

$$Ja = \frac{\rho_l c_{pl}(t_{w,i} - t_{sat})}{\rho_v i_{lv}} \tag{16}$$

For $t_{w,i} - t_{sat}$ = 1 K, from Table 3 it can be observed that, for the evaporating temperatures considered in this work, the frequency of bubble release for R744 is higher than R22 of about 10%.

Also from the analysis of the nucleate boiling contribution predicted by the most known correlations available in literature based on an additive model, it is possible to highlight that the nucleate boiling heat transfer coefficient of carbon dioxide should be greater than that corresponding to the conventional refrigerants. In Table 3 the values of h_{nb} predicted from the correlation of Cooper [35], Jung and Radermacher [36] and Mostinski [37] has been reported for R744 and R22 for q = 10 kW/m²:

$$h_{nb,COOPER} = 55 p_r^{0.12}(-\log_{10} p_r)^{-0.55} M^{-0.5} q^{0.67} \tag{17}$$

$$h_{nb,JUNG\ and\ RADERMACHER} = 207\left(\frac{k_l}{d_d}\right)\left(\frac{q d_d}{k_l t_{sat}}\right)^{0.745}\left(\frac{\rho_v}{\rho_l}\right)^{0.581} Pr_l^{0.533} \tag{18}$$

$$h_{nb,MOSTINSKI} = 0.00147 q^{0.7} p_{cr}^{0.69}(1.8 p_r^{0.17} + 4 p_r^{1.2} + 10 p_r^{10}) \tag{19}$$

In Eq. (18) $d_d = 0.0146\beta\left(\frac{2\sigma}{g(\rho_l - \rho_v)}\right)^{0.5}$ and β is assigned a fixed value of about $\pi/6$, while Eq. (19) must be used with q in W/m² K and p_{cr} in kN/m². From Table 3 it can be observed that h_{nb} for R744 is about three times larger than R22.

With the Sato and Matsumura correlation [38] it can be shown that the vapor quality at which nucleation is fully suppressed is given by the relation:

$$x_{SUP} = \frac{\gamma}{1 + \gamma} \tag{20}$$

where, for a uniform heat flux applied to the wall, γ can be obtain from the relation:

$$\gamma = \left(\frac{\rho_v}{\rho_l}\right)^{0.56}\left(\frac{\mu_l}{\mu_v}\right)^{0.11}\left(\frac{q k_l i_{fg} \rho_v}{98\sigma t_{sat} h_l^2}\right)^{1.11} \tag{21}$$

Using the Dittus–Boelter correlation [20] to evaluate h_l, for G = 200 kg/m² s and q = 10 kW/m², x_{SUP} for R744 is larger (of about 10%) than that corresponding to R22 (Table 3). This is due to the fact that, compared to R22, carbon dioxide presents higher $\frac{\rho_v}{\rho_l}$, k_l, i_{lv}, ρ_v and lower σ. Therefore the nucleate boiling contribution for carbon dioxide is active for a larger range of vapor qualities.

For $t_{sat} \approx 5$ °C the nucleate boiling contribution is enhanced. As a consequence in the region of low vapor quality the nucleate boiling contribution becomes so relevant to determine heat transfer coefficients higher than those pertaining to the region of high vapor quality, while for high vapor quality the heat transfer coefficients remain similar to those corresponding to lower evaporating temperatures.

5.2. Influence of mass flux

From Fig. 4 we can observe that the heat transfer coefficients are nearly independent of mass velocity. This is due to the fact that, as seen above, the convective boiling contribution is not so relevant for carbon dioxide as for others fluids.

5.3. Influence of saturation temperature

As can be noticed from Fig. 4, the heat transfer coefficient at low vapor quality (up to around 30%) increases with a rise of evaporating temperature from $t_{sat} \approx -3$ °C to $t_{sat} \approx 5$ °C; no obvious differences have been observed in the transition from $t_{sat} \approx -8$ °C to $t_{sat} \approx -3$ °C. These trends can be explained taking into account that in the region of low vapor quality the nucleate boiling is the dominant heat transfer mechanism. From Table 3 it can be drew that as the evaporating temperature increases the critical bubble radius decreases and the bubble frequency release increases and, therefore, the nucleate boiling contribution is enhanced. The variations of r_{cr} and f corresponding to the transition between $t_{sat} \approx -3$ °C and $t_{sat} \approx 5$ °C are larger than those pertaining to the transition from $t_{sat} \approx -8$ °C to $t_{sat} \approx -3$ °C. These considerations are also confirmed observing that the nucleate boiling heat transfer coefficient

predicted from the correlations of Cooper [35], Jung and Radermacher [36] and Mostinski [37] becomes about 20% larger when the saturation temperature passes from −3 to 5 °C, while from $t_{sat} \approx -8$ °C to $t_{sat} \approx -3$ °C the increment of h_{nb} is about 10%.

Even if increasing saturation pressure and decreasing refrigerant mass flux x_{SUP} becomes slightly larger (Table 3), no obvious differences have been observed in the value of vapor quality at which the influence of evaporating temperature becomes negligible.

For high vapor quality the heat transfer coefficient is substantially independent from the saturation temperature: this is due to the lower influence of the nucleate boiling as vapor quality increases.

5.4. Influence of heat flux

Fig. 6 shows that a strong dependence of the heat transfer coefficients on the heat flux appears for all values of vapor quality (even if the influence of q at low vapor quality is larger). The effect of heat flux on the heat transfer coefficient shows the dominance of nucleate boiling heat transfer in the whole range of vapor qualities, as expected from the evaluation of x_{SUP}. In fact heat flux has a negligible effect on the convective contribution to heat transfer, while strongly affect nucleate boiling. In particular, as heat flux increases, the liquid superheat Δt becomes higher and, therefore, the critical bubble radius becomes lower [31]. As a consequence, the nucleate boiling contribution increases. Fig. 6 is referred to $G \approx 300$ kg/m^2 s and $t_{sat} \approx 5$ °C, but the above considerations can be extended to the other operating conditions investigated.

6. Comparison with predictive methods and other experimental data

The measured values of heat transfer coefficients have been compared with two of the most important predictive methods specifically developed for carbon dioxide: the phenomenological method of Cheng et al. [23] and the method of Yoon et al. [11].

The comparison has been made both for the whole database and the segregated data by flow regimes (annular and intermittent) and the results are reported in Table 4. To segregate the data by flow regime the flow pattern map by Cheng et al. [22] was used. In the analysis the parameters defined by Eqs. (5)–(7) and the percentage of points inside an error interval of ±30% were evaluated.

For the entire database, it can be observed that the correlations tend to overpredict the experimental data; even if Yoon et al. [11] method returns the best standard deviation (19.9%), Cheng et al. [23] correlation provides the lowest absolute mean error (22.6%) and is able to predict 75.6% of data within ±30% error window. However the above considerations were affected by the data distribution with respect to the flow regimes. The analysis for each flow regime showed different results. In the intermittent region, the method by Yoon et al. [11] granted the more reliable predictions, even if also the method of Cheng et al. [23] returns accurate predictions. Results by Cheng et al. [23] correlation were the best in the annular flow regime both for absolute mean error (10.3%) and standard deviation (13.3%); besides, this method predict 93.1% of data within ±30% error range, while for Yoon et al. [11] correlation results λ = 70.0%.

Table 4
Results of statistical comparison between the predicted and the experimental R744 heat transfer coefficients.

	Number of experimental points	Predictive methods	$\bar{\varepsilon}$ (%)	$\|\varepsilon\|$ (%)	sd (%)	λ (%)
Whole database	217	Cheng et al. [23]	4.7	22.6	30.4	75.6
		Yoon et al. [11]	30.9	31.3	19.9	52.5
Intermittent flow regime	24	Cheng et al. [23]	4.4	4.4	12.6	79.3
		Yoon et al. [11]	3.2	3.2	9.9	81.1
Annular flow regime	152	Cheng et al. [23]	8.6	10.3	13.3	93.1
		Yoon et al. [11]	19.9	20.2	20.1	70.0

Heat transfer coefficients measured in this study have been compared with those obtained by Yun et al. [11] (Fig. 7), Oh et al. [16] (Fig. 8), Cho and Kim [15] and Yoon et al. [17]. The selected works refer to similar sets of operating conditions (tube geometry, surface aspect and disposition; mass fluxes; evaporating temperatures; heat fluxes).

All the authors obtained experimental trends of heat transfer coefficients versus vapor quality similar to those shown in this work; however they hypothesized a partial dryout of liquid film at very low vapor quality. Regarding the absolute values, a good agreement has been observed in most cases, even if some discrepancies have been found; for example, differently from our study, Yun et al. [11] observed: an influence of the heat flux on heat

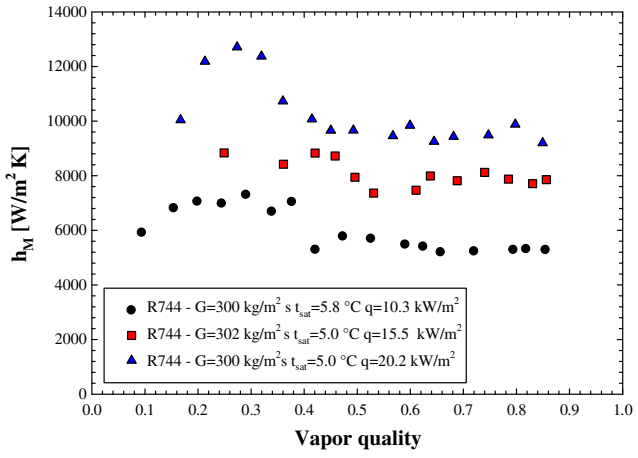

Fig. 6. Local heat transfer coefficients of R744 as a function of vapor quality at varying heat flux for $G \approx 300$ kg/m^2 s and $t_{sat} \approx 5$ °C.

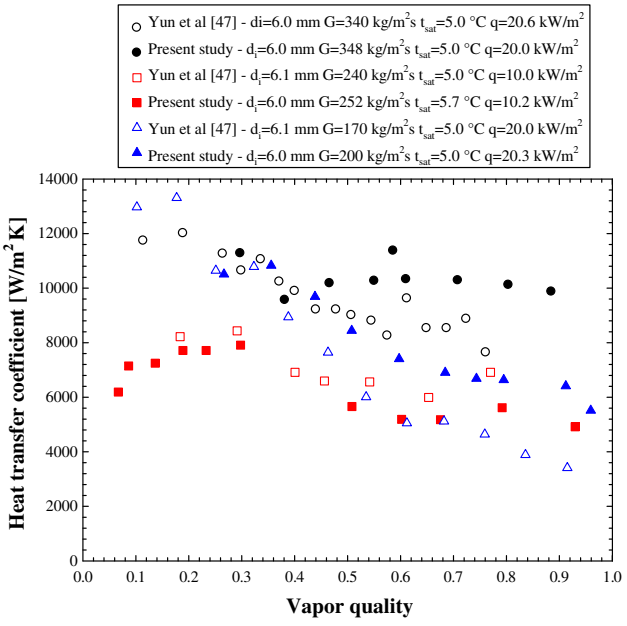

Fig. 7. Comparison of heat transfer coefficients presented in this study with those obtained by Yun et al. [11].

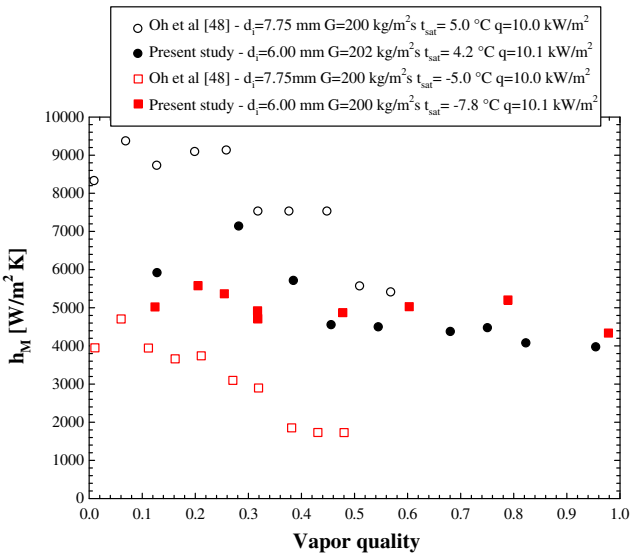

Fig. 8. Comparison of heat transfer coefficients presented in this study with those obtained by Oh et al. [16].

transfer coefficients only for low vapor quality (up to $0.3 \div 0.4$); the heat transfer coefficients increasing with the rise of mass flux for vapor qualities above 0.5 and the decrease with the increase of evaporating temperature at high vapor quality. About the work by Oh et al. [16], even if a limited range of vapor qualities was investigated, important differences in the absolute values can be noticed for $G = 200$ kg/m^2 s, $t_{sat} = -7.8$ °C and $q = 10.1$ kW/m^2 probably due to the slightly greater inner diameter.

From the comparison with Cho and Kim [15] and Yoon et al. [17], it can be observed that the heat transfer coefficients presented in this work are greater even if we used an inner diameter lower. Besides Cho and Kim [15] measured heat transfer coefficients increasing at increasing mass flux.

7. Conclusions

The scheduled phase out of *HCFC* refrigerants has prompted the refrigeration industry to identify new possible alternative. Carbon dioxide is gaining renewed interest as an environmentally safe refrigerant. In order to improve the energy efficiency of R744 systems, an accurate knowledge of heat transfer coefficients during evaporation is fundamental.

Some studies have been carried out in recent years to measure the CO_2 two-phase heat transfer coefficients during flow boiling in horizontal circular macrochannels. Nevertheless more accurate local heat transfer data are still needed. In fact data from different studies available in literature show somehow different values of heat transfer coefficients at similar operating conditions. Besides the influence of mass flux, evaporating temperature, heat flux and vapor quality on the heat transfer coefficients is not completely cleared.

In this paper experimental heat transfer coefficients for R744 during flow boiling in a smooth, horizontal, circular, stainless steel tube with 6.00 mm inner diameter are presented. The tests were carried out by means of a new experimental apparatus developed for accurate carbon dioxide measurements. The reliability of the measurements was verified through accurate preliminary tests that showed an instrumentation calibration and overall system performance consistent with the desired accuracy.

We obtained 184 experimental points in 18 operating conditions commonly encountered in dry-expansion evaporators. The experiments showed that the heat transfer coefficients are nearly independent of mass velocity and, for low evaporating temperatures, of vapor quality. The influence of evaporating temperature is remarkable only for low vapor quality. A remarkable influence of the heat flux on the heat transfer coefficients for all values of vapor quality has been also observed.

Taking into account that the heat transfer process depends on the liquid and vapor phase distributions, an accurate analysis of the flow regimes corresponding to the experimental points based on the local circumferential distribution of heat transfer coefficients has been carried out.

At low vapor qualities, from the experimental data analysis, the slug flow regime seems to occur and the top of the tube shows the highest local heat transfer coefficient. This is due to the fact that in the liquid film region at the top of the tube the nucleate boiling is larger.

At higher values of vapor quality the flow regime becomes stratified-wavy or annular depending on the mass flux. Differently from the stratified-wavy regime, in the annular flow region no obvious variation of circumferential heat transfer coefficient was observed. This implies that dryout does not arise. Besides, compared to the flow pattern map of Cheng et al. [22,23], in our experiments the transition from slug to stratified-wavy/annular flow regime seems to take place at slightly higher values of vapor quality and the transition from stratified-wavy and annular flow regime seems to occur for slightly higher mass flux.

The results were compared against the methods of Cheng et al. [23] and Yoon et al. [11]: the statistical analysis showed that the Cheng et al. [23] correlation provides the best results.

References

[1] EC Regulation 2037/2000, 2000.
[2] The Kyoto Protocol to the United Nations Framework Convention on Climate Change, 1997.
[3] Directive 2006/40/EC, 2006.
[4] J.M. Calm, Options and outlook for chiller refrigerants, International Journal of Refrigeration 25 (2002) 705–715.
[5] G. Lorentzen, The use of natural refrigerants: a complete solution to the CFC/*HCFC* predicament, International Journal of Refrigeration 18 (1995) 190–197.
[6] M.-H. Kim, J. Pettersen, C.W. Bullard, Fundamental process and system design issues in CO_2 vapor compression systems, Progress in Energy and Combustion Science 30 (2004) 119–174.
[7] A. Cavallini, C. Zilio, Carbon dioxide as a natural refrigerant, in: Proceedings of the 5th International Congress on Sustainable Energy Technologies, Vicenza, Italy, 2006.
[8] J.R. Thome, G. Ribatski, State-of-the-art of two-phase flow and flow boiling heat transfer and pressure drop of CO_2 in macro- and micro-channels, International Journal of Refrigeration 28 (2006) 1–20.
[9] A. Bredesen, A. Hafner, J. Pettersen, P. Neksa, K. Aflekt, Heat transfer and pressure drop for in-tube evaporation of CO_2, in: Proceedings of the International Conference in Heat Transfer Issues in Natural Refrigerants, University of Maryland, USA, 1997, pp. 1–15.
[10] H.J. Knudsen, R.H. Jensen, Heat transfer coefficient for boiling carbon dioxide, in: Workshop Proceedings – CO_2 Technologies in Refrigeration, Heat Pumps and Air Conditioning Systems, Trondheim, Norway, 1997, pp. 319–328.
[11] R. Yun, Y. Kim, M.S. Kim, Y. Choi, Boiling heat transfer and dryout phenomenon of CO_2 in a horizontal smooth tube, International Journal of Heat and Mass Transfer 46 (2003) 2353–2361.
[12] C.Y. Park, P.S. Hrnjak, Flow boiling heat transfer of CO_2 at low temperatures in a horizontal smooth tube, Journal of Heat Transfer 127 (2005) 1305–1312.
[13] C.Y. Park, P.S. Hrnjak, Evaporation of CO_2 in a horizontal smooth tube, in: IIR 2005 Vicenza Conference-Thermophysical Properties and Transfer Processes of Refrigerants, Vicenza, Italy, 2005, pp. 225–236.
[14] E. Hihara, Fundamental technology for carbon dioxide operated heat pumps, in: JSAE Automotive Air-Conditioning Symposium, 2006, pp. 243–262.
[15] J.M. Cho, M.S. Kim, Experimental studies on the evaporative heat transfer and pressure drop of CO_2 in smooth and micro-fin tubes of the diameters of 5 and 9.52 mm, International Journal of Refrigeration 30 (2007) 986–994.
[16] H.-K. Oh, H.-G. Ku, G.-S. Roh, C.-H. Son, S.-J. Park, Flow boiling heat transfer characteristics of carbon dioxide in a horizontal tube, Applied Thermal Engineering 28 (2008) 1022–1030.
[17] S.H. Yoon, E.S. Cho, Y.W. Hwang, M.S. Kim, K. Min, Y. Kim, Characteristics of evaporative heat transfer and pressure drop of carbon dioxide and correlation development, International Journal of Refrigeration 27 (2004) 111–119.
[18] E.W. Lemmon, M.O. Mc Linden, M.L. Huber, NIST Standard Reference Database 23, Version 7.0, Physical and Chemical Properties.

[19] R.J. Moffat, Describing uncertainties in experimental results, Experimental Thermal Fluid Sciences 1 (1988) 3–17.
[20] F.W. Dittus, L.M.K. Boelter, Heat transfer in automobile radiator of the tubular type, University of California Publications on Engineering 2 (1930) 443–461.
[21] V. Gnielinski, New equations for heat and mass transfer in turbulent pipe and channel flow, International Chemical Engineering 16 (1976) 359–368.
[22] L. Cheng, G. Ribatski, J. Moreno Quibén, J.R. Thome, New prediction methods for CO_2 evaporation inside tubes: Part I – A two-phase flow pattern map and a flow pattern based phenomenological model for two-phase flow frictional pressure drops, International Journal of Heat and Mass Transfer 51 (2008) 111–124.
[23] L. Cheng, G. Ribatski, J.R. Thome, New prediction methods for CO_2 evaporation inside tubes: Part II – An updated general flow boiling heat transfer model based on flow patterns, International Journal of Heat and Mass Transfer 51 (2008) 125–135.
[24] L. Wojtan, T. Ursenbacher, J.R. Thome, Investigation of flow boiling in horizontal tubes: Part I – A new diabatic two-phase flow pattern map, International Journal of Heat and Mass Transfer 48 (2005) 2955–2969.
[25] L. Wojtan, T. Ursenbacher, J.R. Thome, Investigation of flow boiling in horizontal tubes: Part II – Development of a new heat transfer model for stratified-wavy, dry-out and mist flow regimes, International Journal of Heat and Mass Transfer 48 (2005) 2970–2985.
[26] D. Steiner, Heat transfer to boiling saturated liquids, VDI Wärmeatlas (VDI Heat Atlas), in: Verein Deutscher Ingenieure (Ed.), VDI-Gessellschaft Verfahrenstechnik und Chemie-ingenieurwesen (GCV), Translator: J.W. Fullarton, Düsseldorf, 1993.
[27] D. Biberg, An explicit approximation for the wetted angle in two-phase stratified pipe flow, Canadian Journal of Chemical Engineering 77 (1999) 1221–1224.
[28] G. Sun, G.F. Hewitt, V.V. Wadekar, A heat transfer model for slug flow in a horizontal tube, International Journal of Heat and Mass Transfer 47 (2004) 2807–2816.
[29] H. Mori, S. Yoshida, K. Ohishi, Y. Kokimoto, Dryout quality and post dryout heat transfer coefficient in horizontal evaporator tubes, in: Proceedings of the 3rd European Thermal Sciences Conference, 2000, pp. 839–844.
[30] N. Kattan, J.R. Thome, D. Favrat, Flow boiling in horizontal tubes. Part 3: Development of a new heat transfer model based on flow patterns, Journal of Heat Transfer 120 (1998) 156–165.
[31] V.P. Carey, Liquid–Vapor Phase-Change Phenomena An Introduction to the Thermophysics of Vaporization and Condensation Processes in Heat Transfer Equipment, Hemisphere, New York, 1991.
[32] N. Zuber, Nucleate boiling – the region of isolated bubbles – similarity with natural convection, International Journal of Heat and Mass Transfer 6 (1963) 53–65.
[33] M.K. Jensen, G.J. Memmel, Evaluation of bubble departure diameter correlations, in: Proceedings of the Eighth International Heat Transfer Conference, 1986, pp. 1907–1912.
[34] S.S. Kutateladze, I.I. Gogonin, Growth rate and detachment diameter of a vapor bubble in free convection boiling in saturated liquids, High Temperature 17 (1979) 667–671.
[35] M.K. Cooper, Saturated nucleate pool boiling: a simple correlation, in: First UK National Heat Transfer Conference, 1984, pp. 785–793.
[36] D.S. Jung, R. Radermacher, Prediction of heat transfer coefficient for various refrigerants during evaporation, Paper No. 3492, ASHRAE Annual Meeting, Indianapolis, June, 2002.
[37] I.L. Mostinski, Application of the rule of corresponding states for calculation of heat transfer and critical heat flux, Teploenergetika 4 (1963) 66.
[38] T. Sato, H. Matsumura, Bullettin of the Japan Society of Mechanical Engineering 7 (1964) 392.